Semisupervised Learning of Hierarchical Latent Trait Models for Data Visualization

Ian T. Nabney, Yi Sun, Peter Tiňo, and Ata Kabán

Abstract—Recently, we have developed the hierarchical Generative Topographic Mapping (HGTM), an interactive method for visualization of large high-dimensional real-valued data sets. In this paper, we propose a more general visualization system by extending HGTM in three ways, which allows the user to visualize a wider range of data sets and better support the model development process. 1) We integrate HGTM with noise models from the exponential family of distributions. The basic building block is the Latent Trait Model (LTM). This enables us to visualize data of inherently discrete nature, e.g., collections of documents, in a hierarchical manner. 2) We give the user a choice of initializing the child plots of the current plot in either *interactive*, or *automatic* mode. In the interactive mode, the user selects "regions of interest," whereas in the automatic mode, an unsupervised minimum message length (MML)-inspired construction of a mixture of LTMs is employed. The unsupervised construction is particularly useful when high-level plots are covered with dense clusters of highly overlapping data projections, making it difficult to use the interactive mode. Such a situation often arises when visualizing large data sets. 3) We derive general formulas for magnification factors in latent trait models. Magnification factors are a useful tool to improve our understanding of the visualization plots, since they can highlight the boundaries between data clusters. We illustrate our approach on a toy example and evaluate it on three more complex real data sets.

Index Terms—Hierarchical model, latent trait model, magnification factors, data visualization, document mining.

1 Introduction

Topographic visualization of multidimensional data has been an important method of data analysis and data mining for several years [4], [18]. Visualization is an effective way for domain experts to detect clusters, outliers, and other important structural features in data. In addition, it can be used to guide the data mining process itself by giving feedback on the results of analysis [23]. In this paper, we use latent variable models to visualize data, so that a single plot may contain several data clusters; our aim is to provide sufficiently informative plots that the clusters can be *seen* to be distinct rather than confining each model to a single cluster (as would be appropriate for cluster analysis).

In a complex domain, however, a single two-dimensional projection of high-dimensional data may not be sufficient to capture all of the interesting aspects of the data. Therefore, hierarchical extensions of visualization methods [7], [22] have been developed. These allow the user to "drill down" into the data; each plot covers a smaller region and it is therefore easier to discern the structure of the data. Also, plots may be at an angle and so reveal more information. For example, clusters may be split apart instead of lying on top of each other.

Recently, we have developed a general and principled approach to the interactive construction of nonlinear visualization hierarchies [27], the basic building block of which is the Generative Topographic Mapping (GTM) [4]. GTM is a probabilistic reformulation of the self-organizing map (SOM) [17] in the form of a nonlinear latent variable model with a spherical Gaussian noise model.

The extension of the GTM algorithm to discrete variables was described in [5] and a generalization of this to the Latent Trait Model (LTM), a latent variable model class whose noise models are selected from the exponential family of distributions, was developed in [14]. In this paper, we extend the hierarchical GTM (HGTM) visualization system to incorporate LTMs. This enables us to visualize data of an inherently discrete nature, e.g., collections of documents.

A hierarchical visualization plot is built in a recursive way; after viewing the plots at a given level, the user may add further plots at the next level down in order to provide more insight. These child plots can be trained using the EM algorithm [10], but their parameters must be initialized in some way. Existing hierarchical models do this by allowing the user to select the position of each child plot in an *interactive* mode; see [27]. In this paper, we show how to provide the user with an *automatic* initialization mode which works within the same principled probabilistic framework as is used for the overall hierarchy. The automatic mode allows the user to determine both the number and the position of child LTMs in an *unsupervised* manner. This is particularly valuable when dealing with large quantities of data that make visualization plots at higher levels complex and difficult to deal with in an interactive manner.

An intuitively simple but flawed approach would be to use a data partitioning technique (e.g., [25]) for segmenting the data set, followed by constructing visualization plots in the individual compartments. Clearly, in this case, there would be no direct connection between the criterion for

- *I.T. Nabney is with the Neural Computing Research Group, Aston University, Birmingham, B4 7ET, United Kingdom. E-mail: i.t.nabney@aston.ac.uk.*
- *Y. Sun is with the School of Computer Science, University of Hertfordshire, Hatfield, Herts AL10 9AB, United Kingdom. E-mail: Y.2.Sun@herts.ac.uk.*
- *P. Tiňo and A. Kabán are with the School of Computer Science, University of Birmingham, Birmingham B15 2TT, United Kingdom. E-mail: {P.Tino, A.Kaban}@cs.bham.ac.uk.*

Manuscript received 13 Nov. 2002; revised 22 Oct. 2003; accepted 19 July 2004.
For information on obtaining reprints of this article, please send e-mail to: tkde@computer.org, and reference IEEECS Log Number 117773.

choosing the quantization regions and that of making the local low-dimensional projections. By employing LTM, however, such a connection can be established in a principled manner. This is achieved by exploiting the probabilistic nature of the model, which enables us to use a principled minimum message length (MML)-based learning of mixture models with an embedded model selection criterion. This approach has been used for Gaussian mixture models [11].[1] Hence, given a parent LTM, the number and position of its children is based on the modeling properties of the children themselves—without any ad hoc criteria which would be exterior to the model.

Previous experience has indicated that magnification factors may provide valuable additional information to the user's understanding of the visualization plots, since they can highlight the boundaries between data clusters. In [6], formulas for magnification factors were only derived for the GTM. In this paper, we derive formulas for magnification factors in full generality for latent trait models.

In the next section, we briefly review the latent trait model. In Section 3, a hierarchical latent trait model is developed. Section 4 presents the model selection criterion based on minimum message length that we apply to mixtures of LTMs. Section 5 presents and discusses experimental results and compares them with existing methods. We derive a general formula for magnification factors in LTMs in Section 6. Finally, Section 7 summarizes the key contributions of the paper.

2 The Latent Trait Model (LTM)

Latent trait models [14] are generative models which are powerful and principled tools for data analysis and visualization. As a generalization of the Generative Topographic Mapping (GTM) [4], the latent trait model family [14] offers a framework which includes the definition of appropriate probability models for discrete observations.

Consider an L-dimensional *latent space* $\mathcal{H}$, which, for visualization purposes, is typically a bounded 2D Euclidean domain, e.g., the square $[-1,1]\times[-1,1]$. The aim is to represent multidimensional data vectors $\{\mathbf{t}_n\}_{n=1,\ldots,N}$ using the latent space so that "important" structural characteristics are revealed. A nonlinear function maps the latent space to the data space $\mathcal{D}=\Re^D$. The latent plane (assuming a two-dimensional latent space) becomes a (nonlinear) 2D manifold in the high-dimensional data space.

For tractability, the latent space is discretized by introducing a regular array (or grid) of K latent points $\boldsymbol{x}_k\in\mathcal{H}, k=1,\ldots,K$ (which are analogous to the nodes of the SOM [18]). A uniform prior distribution is imposed over the latent points $\boldsymbol{x}_k$, leading to the following expression for the unconditional data density of an observed data point $\mathbf{t}\in\Re^{\mathbf{D}}$

$$p(\mathbf{t})=\sum_{k=1}^{K}p(\mathbf{t}|\boldsymbol{x}_k)p(\boldsymbol{x}_k)=K^{-1}\sum_{k=1}^{K}p(\mathbf{t}|\boldsymbol{x}_k). \quad (1)$$

The conditional data distribution, $p(\mathbf{t}|\boldsymbol{x}_k)$, (conditioned on the kth latent space point $\boldsymbol{x}_k\in\mathcal{H}$) is modelled as a member of the exponential family in a parameterized functional form [2]

$$p_B(\mathbf{t}|\boldsymbol{x}_k,\Theta)=\exp\{\boldsymbol{f}_{\Theta}(\mathbf{x}_k)\mathbf{t}-B(\boldsymbol{f}_{\Theta}(\boldsymbol{x}_k))\}p_0(\mathbf{t}). \quad (2)$$

Here, Θ is the parameter vector of the model, $B(\boldsymbol{f}_{\Theta}(\mathbf{x}_k))=\ln\int\exp(\boldsymbol{f}_{\Theta}(\boldsymbol{x}_k)\mathbf{t})p_0(\mathbf{t})\,d\mathbf{t}$ denotes the cumulant generating function of $p(\mathbf{t}|\boldsymbol{x}_k)$, and $p_0(\mathbf{t})$ is a factor independent of Θ. Recall that the exponential family includes the Gaussian and Student t-distributions and also discrete random variables such as the Bernoulli and multinomial distributions.

The function $\boldsymbol{f}(\cdot)$ represents a smooth mapping from latent to data space; in order to make training fast, $\boldsymbol{f}$ has the form of a General Linear Regression model, and is defined by $\boldsymbol{f}_{\Theta}(\boldsymbol{x}_k)=\Theta\boldsymbol{\phi}(\boldsymbol{x}_k)$, where $\Theta\in\Re^{D\times M}$ is a parameter matrix and $\boldsymbol{\phi}(\cdot)=(\phi_1(\cdot),\ldots,\phi_M(\cdot))^T, \phi_m(\cdot):\mathcal{H}\rightarrow\Re$, is a fixed set of M nonparametric nonlinear basis functions. These could be any smooth functions; typically, Gaussian radial basis functions are employed. A linear basis function $\phi_0(x)=1,\forall x$, may be included to account for the bias term (which is set to the data mean). The notation $\boldsymbol{\phi}_k=\boldsymbol{\phi}(\boldsymbol{x}_k)$ will be used as a shorthand.

A latent trait model with fixed parameters Θ defines a density in the data space,

$$\boldsymbol{z}:\mathcal{H}\rightarrow\Re^D,\quad \boldsymbol{z}(\boldsymbol{x}_k)=\boldsymbol{b}(\Theta\Phi(\boldsymbol{x}_k))=\boldsymbol{b}(\Theta\boldsymbol{f}(\boldsymbol{x}_k)). \quad (3)$$

This probabilistic interpretation is fundamental to our approach to constructing a hierarchy of models. We refer to the manifold $\boldsymbol{f}(\mathcal{H})$ as the *projection manifold* of the LTM.

LTMs are trained to maximize the likelihood of the training set $\zeta=\{\mathbf{t}_1,\ldots,\mathbf{t}_N\}$ using an EM algorithm [10], the M-step of which consists of solving the equation

$$\mathbf{T}\mathbf{R}^T\boldsymbol{\Phi}^T=\mathbf{b}(\boldsymbol{\Theta}\boldsymbol{\Phi})G\boldsymbol{\Phi}^T \quad (4)$$

for $\boldsymbol{\Theta}$, where the function $\mathbf{b}(\cdot)$ denotes the gradient of the cumulant function $B(\cdot)$,[2] $\boldsymbol{\Phi}$ is an $M\times K$ matrix with ϕ_k in its kth column, $\mathbf{T}$ is the data matrix including N data vectors $\{\mathbf{t}_n\}$ as columns, $\mathbf{R}=(R_{kn})_{k=1,\ldots,K,n=1,\ldots,N}$ and G is a diagonal matrix with elements $g_{kk}=\sum_{n=1}^{N}R_{kn}$, where R_{kn}, computed via Bayes' theorem in the E-step,

$$R_{kn}=p(\boldsymbol{x}_k|\mathbf{t}_n)=\frac{p(\mathbf{t}_n|\boldsymbol{x}_k,\boldsymbol{\Theta})p(\boldsymbol{x}_k)}{\sum_{k'=1}^{K}p(\mathbf{t}_n|\boldsymbol{x}_{k'},\boldsymbol{\Theta})p(\boldsymbol{x}_{k'})}, \quad (5)$$

is the "responsibility" of the latent point $\boldsymbol{x}_k$ for generating $\mathbf{t}_n$. The E-step and M-step are iterated until the change in likelihood falls below a user-defined threshold.

Once trained, the LTM can be used for visualization. To do this, the map $\boldsymbol{f}$ has to be "inverted" so that there is a latent space point corresponding to each data point. The latent space representation of a point $\mathbf{t}_n$ is taken to be the mean of the posterior distribution $p(\boldsymbol{x}_k|\mathbf{t}_n)$ over the latent space. This can be computed using (5) and averaging $\boldsymbol{x}_k$ weighted by R_{kn} over k.

1. This framework uses Jeffrey's priors, which implies that the estimation of the model parameters is equivalent to a maximum likelihood (ML) formulation. The MML criterion penalizes overly complex models, but does *not* regularize the model parameters themselves.

2. It is the inverse link function [21] of the noise distribution.

3 A General Framework for Hierarchical Latent Trait Models

When dealing with large and complex data sets, a single global visualization plot is often not sufficient to get a good understanding of the relationships in the data. In order to represent complex intrinsic information when visualizing large data sets, hierarchical visualization systems have been proposed and developed in the literature, [7], [27]. In [7], a locally linear hierarchical visualization system was defined. We have recently extended this system to hierarchies of nonlinear GTM projection manifolds in [27]. This paper showed that in many cases, the use of a nonlinear latent space model significantly reduced the number of visualization plots required to get good intercluster separation and represent the data structure.

In this section, we provide a general formulation of hierarchical latent trait mixture models. The benefit of this to the user is that a wider range of conditional density models $p_B(\mathbf{t}|x_k, \mathbf{\Theta})$ can be used. For example, binary data can be visualized using a Bernoulli distribution [14]. If the data contains outliers, a Student *t*-distribution may be more appropriate than the Gaussian used in HGTM. Preliminary results of organizing LTMs into a hierarchy have been encouraging [15], and motivated the work described in this paper.

The hierarchical LTM arranges a set of LTMs and their corresponding plots in a tree structure $\mathcal{T}$. The *Root* is at level 1, children of level-ℓ models are at level $\ell + 1$.

Each model $\mathcal{M}$ in the hierarchy, except for *Root*, has an associated parent-conditional mixture coefficient, or prior, $\pi(\mathcal{M}|Parent(\mathcal{M}))$. The priors are nonnegative and satisfy the consistency condition: $\sum_{\mathcal{M}\in Children(\mathcal{N})} \pi(\mathcal{M}|\mathcal{N}) = 1$. Unconditional priors for the models are recursively calculated as follows: $\pi(Root) = 1$, and for all other models

$$\pi(\mathcal{M}) = \prod_{i=2}^{Level(\mathcal{M})} \pi(Path(\mathcal{M})_i | Path(\mathcal{M})_{i-1}), \tag{6}$$

where $Path(\mathcal{M}) = (Root, \ldots, \mathcal{M})$ is the $\mathcal{P}$-tuple of nodes defining the path of length $\mathcal{P}$ in $\mathcal{T}$ from *Root* to $\mathcal{M}$.

The leaves($\mathcal{T}$) of the tree are defined to be the set of nodes of $\mathcal{T}$ without children. The distribution defined by the hierarchical model is a mixture of distributions defined by the leaves of $\mathcal{T}$

$$P(\mathbf{t}|\mathcal{T}) = \sum_{\mathcal{M}\in Leaves(\mathcal{T})} \pi(\mathcal{M}) P(\mathbf{t}|\mathcal{M}). \tag{7}$$

Nonleaf models have two roles in the hierarchy:

1. Every model is a leaf model at some point during the construction of the hierarchy.
2. Nonleaf models are useful for determining the relationship between subplots in the hierarchy.

3.1 Training

The hierarchical LTM is trained using EM to maximize its likelihood with respect to the data sample $\zeta = \{\mathbf{t}_1, \mathbf{t}_2, \ldots, \mathbf{t}_N\}$. Training of a hierarchy of LTMs proceeds in a recursive fashion. First, the *Root* LTM is trained and used to visualize the data. Then, the user identifies interesting regions on the visualization plot that they would like to model in a greater detail.

Having trained models $\mathcal{N}$ at level ℓ, the expectation of the complete data likelihood of level-$(\ell+1)$ is

$$< \mathcal{L}_{comp}^{\ell+1} > = \sum_{n=1}^{N} \sum_{\mathcal{N}\in Nodes(l)} P(\mathcal{N}|\mathbf{t}_n) \sum_{\mathcal{M}\in Children(\mathcal{N})} P(\mathcal{M}|\mathcal{N}, \mathbf{t}_n) \sum_{k=1}^{K_\mathcal{M}} R_{kn}^{\mathcal{M}} \ln\{\pi(\mathcal{N})\pi(\mathcal{M}|\mathcal{N}) P(\mathbf{t}_n, \boldsymbol{x}_k^{\mathcal{M}})\}. \tag{8}$$

3.1.1 E-Step

In the E-step, we estimate the posterior distribution of all hidden variables, using the "old" values of LTM parameters. Given a data point $\mathbf{t}_n$, we compute the model responsibilities corresponding to the competition among models belonging to the same parent as

$$P(\mathcal{M}|Parent(\mathcal{M}), \mathbf{t}_n) = \frac{\pi(\mathcal{M}|Parent(\mathcal{M})) P(\mathbf{t}_n|\mathcal{M})}{\sum_{\mathcal{M}'\in[\mathcal{M}]} \pi(\mathcal{M}'|Parent(\mathcal{M})) P(\mathbf{t}_n|\mathcal{M}')}, \tag{9}$$

where

$$[\mathcal{M}] = Children(Parent(\mathcal{M})). \tag{10}$$

Imposing $P(Root|\mathbf{t}_n) = 1$, the unconditional (on parent) model responsibilities are recursively determined by

$$P(\mathcal{M}|\mathbf{t}_n) = P(\mathcal{M}|Parent(\mathcal{M}), \mathbf{t}_n) P(Parent(\mathcal{M})|\mathbf{t}_n). \tag{11}$$

Responsibilities of the latent space centers $\boldsymbol{x}_k^{\mathcal{M}}$, $k = 1, 2, \ldots, K_\mathcal{M}$, corresponding to the competition among the latent space centers in each model $\mathcal{M}$, are calculated using (5).

3.1.2 M-Step

In the M-step, we estimate the parameters using the posterior over hidden variables computed in the E-step.

Parent-conditional mixture coefficients are determined using

$$\pi(\mathcal{M}|Parent(\mathcal{M})) = \frac{\sum_{n=1}^{N} P(\mathcal{M}|\mathbf{t}_n)}{\sum_{n=1}^{N} P(Parent(\mathcal{M})|\mathbf{t}_n)}. \tag{12}$$

Parameters $\mathbf{\Theta}^{(\mathcal{M})}$ of the LTM $\mathcal{M}$ are calculated by solving

$$\mathbf{T}\mathbf{R}^{(\mathcal{M})T}\mathbf{\Phi}^T = \mathbf{b}(\mathbf{\Theta}^{(\mathcal{M})}\mathbf{\Phi}) G^{(\mathcal{M})}\mathbf{\Phi}^T, \tag{13}$$

where $\mathbf{R}^{(\mathcal{M})} = (R_{kn}^{\mathcal{M}})_{k=1,\ldots,K,n=1,\ldots,N}$. $R_{kn}^{\mathcal{M}}$ are scaled (by (11)) responsibilities (5), $R_{kn}^{\mathcal{M}} = P(\mathcal{M}|\mathbf{t}_n) R_{kn}$; $G^{(\mathcal{M})}$ is a diagonal matrix with elements $g_{kk}^{\mathcal{M}} = \sum_{n=1}^{N} R_{kn}^{\mathcal{M}}$.

When solving (13), if the link function $\mathbf{b}(\cdot)$ is the identity, one gets the closed form M-step of HGTM[3] [27], but, in general, a nonlinear optimization algorithm is required. In

3. Even though we treat GTM as a special case of LTM with spherical Gaussian noise model, (2) does not account for the "width" parameter. We decided to use the simplified formulation (2), because it is sufficient for all other interesting noise models, such as Bernoulli, Poisson, multinomial, etc. In the case of spherical Gaussian noise model, solving (13) sets the means of the Gaussians and the width parameter needs to be updated as in [27].

the simplest case, we may employ a gradient-based inner loop M-step[4]

$$\Delta \Theta^{(\mathcal{M})} \propto \left\{ \mathbf{T}\mathbf{R}^{(\mathcal{M})T} - \mathbf{b}(\Theta^{(\mathcal{M})}\Phi) G^{(\mathcal{M})} \right\} \Phi. \qquad (14)$$

Training times are dependent on the data set and the number of levels in the hierarchy. For the examples presented in this paper (of up to 8,000 data points), training times for the complete hierarchy were in the order of 2-4 hours for a 1GHz Linux PC running MATLAB. For data of a fixed complexity, the algorithm scales linearly in the number of examples and the dimensionality of the data space. Note that visualization of a large data set using a trained model is relatively quick (less than a minute). Because our model can generalize, it is always possible to train it on a smaller subset of the data and, thus, to tackle very large data sets in practice.

3.2 Model Initialization

When initializing submodels, there are two things to determine: the number of submodels and the initial parameters of the submodels. We view the problem of initializing submodel parameters primarily as one of locating which region of data space each submodel should be responsible for. To do this, regions of interest are defined by the user in the latent (visualization) space. The points $\mathbf{c}_i$ selected in the latent space $\mathcal{H}$ correspond to the "centers" of these regions.

These "centers" of the "regions of interest" are mapped back to the data space and Voronoi compartments [1] defined by the mapped points $z(\mathbf{c}_i) \in \mathcal{D}$, where z is the map (3) of the corresponding LTM, are calculated in the data space. In the case of a Gaussian noise model, the child LTMs are initialized by local PCA in the corresponding Voronoi compartments [27]. When using other noise models such as Bernoulli or multinomial distributions, the PCA-initialized LTMs are, in addition, individually trained (Section 2) in their corresponding Voronoi compartments for 1 EM iteration. The EM iteration "settles" the component LTMs to their corresponding modeling regions. Empirically, this initialization strategy works very well. We perform this additional initialization step when the PCA initialization alone does not "match" the noise distribution well, e.g., when the noise distribution is nonsymmetric or the data space is discrete.

After the initialization of each child model, the full hierarchical training described in Section 3.1 is used.

3.3 Plotting the Projections

We adopt the strategy used in [7], [27] and take advantage of the probabilistic nature of our model by plotting projections of all the data points on every plot, but modifying the intensity in proportion to the responsibility $P(\mathcal{M}|\, \mathbf{t}_n)$ (11) which each plot (submodel $\mathcal{M}$) has for the data point $\mathbf{t}_n$. Points that are not well captured by a particular plot will appear with low intensity.

4. In this partial M-step, we could alternatively use iterative reweighted least squares [35].

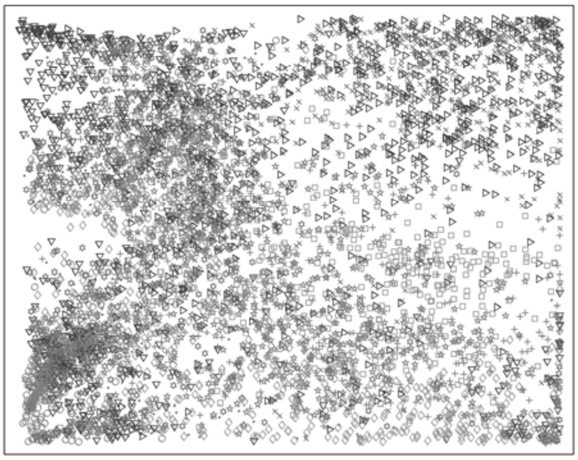

Fig. 1. An example of strongly overlapping clusters: visualization of a collection of documents with a single Latent Trait Model. The documents are classified according to the topic they cover. Each of 10 topic classes is assigned a unique marker.

4 Unsupervised Learning of Mixtures of LTMs

In previous sections, we have developed a general framework for a visualization hierarchy. The user selects the "regions of interest" to select initial locations of child models and extend the visualization hierarchy. This method is powerful when the clusters are separated clearly in the two-dimensional latent space. On the other hand, when facing a cluttered plot like that in Fig. 1, where thousands of data points are shown (with densely clustered and overlapping projections), the user may be unable to determine where submodels should be placed. In order to resolve this problem, we have developed an alternative initialization algorithm which decides both the number of submodels and their location automatically. As far as we are aware, there is no other algorithm for automatic initialization of subplots in a hierarchical visualization model. In this section, we will focus solely on the algorithm for mixture models.

4.1 MML Formulation for Unsupervised Learning of Mixture Models

Given a set $\zeta = \{\mathbf{t}_1, \mathbf{t}_2, \ldots, \mathbf{t}_N\}$ of data points, minimum message length (MML) strategies select, among the models inferred from ζ, the one which minimizes length of the message transmitting ζ [28]. Given that the data is modeled by a parametric probabilistic model $P(\zeta|\boldsymbol{\theta})$, the message consists of two parts—one specifying the model parameters, the other specifying the data given the model: $\mathrm{Length}(\boldsymbol{\theta}, \zeta) = \mathrm{Length}(\boldsymbol{\theta}) + \mathrm{Length}(\zeta|\boldsymbol{\theta})$.

The MML principle was first applied to unsupervised learning of mixture models in [29] and was extended to hierarchical models in [8]. A computer program, Snob, that uses these principles for both parameter estimation and model selection was described in [30]; this provides a flat clustering model. The hierarchical model used in these papers differs from ours in three main ways. First, only the leaf nodes define a probability density, while our hierarchy defines a density at all levels. Second, the earlier model has relatively simple distribution models for clustering, while we allow more complex component models (LTMs) which support visualization. Third, a heuristic algorithm is used to train the hierarchy, while we use EM.

Recently, Figueiredo and Jain [11] have developed an MML framework for unsupervised learning of mixture models; with the choice of a Jeffrey's prior, the algorithm selects the "appropriate" number of components while the parameters of each model are estimated by ML. (A similar approach for other density models was formulated in [30] and [32].) The novelty of their proposed approach is that parameter estimation and model selection are integrated in a single EM algorithm, rather than using a model selection criterion on a set of preestimated candidate models.

The particular form of MML criterion adopted in [11] is of the form $\hat{\boldsymbol{\theta}} = \underset{\boldsymbol{\theta}}{\operatorname{argmin}} \mathcal{L}(\boldsymbol{\theta}, \zeta)$, where

$$\mathcal{L}(\boldsymbol{\theta}, \zeta) = -\log P(\boldsymbol{\theta}) - \log P(\zeta|\boldsymbol{\theta}) + \frac{1}{2}\log|\mathbf{I}(\boldsymbol{\theta})| + \frac{c}{2}\left(1 + \log\frac{1}{12}\right), \tag{15}$$

where $\mathbf{I}(\boldsymbol{\theta})$ is the expected Fisher information matrix, $|\mathbf{I}(\boldsymbol{\theta})|$ is its determinant, and c is the number of free parameters, i.e., the dimension of $\boldsymbol{\theta}$. This approach was first proposed in [33].

By imposing a noninformative Jeffreys' prior [3] on both the vector of mixing coefficients $\{\pi(\mathcal{M})\}$ and the parameters $\boldsymbol{\Theta}^{(\mathcal{M})}$ of individual mixture components [11], (15) becomes

$$\mathcal{L}(\boldsymbol{\theta}, \zeta) = \frac{Q}{2} \sum_{\pi(\mathcal{M})>0} \log\left(\frac{N \cdot \pi(\mathcal{M})}{12}\right) + \frac{A}{2}\log\frac{N}{12} + \frac{A(Q+1)}{2} - \log P(\zeta|\boldsymbol{\theta}), \tag{16}$$

where A is the number of mixture components with positive prior $\pi(\mathcal{M}) > 0$ and Q is the number of free parameters of each individual mixture component. The use of a noninformative prior is mathematically convenient, since it cancels out the Fisher information matrix term $\mathbf{I}(\boldsymbol{\theta})$, which is complex to analyze and very expensive to compute. However, such a prior is formally equivalent to a Bayesian prior which favors parameter values around the values where the model is most sensitive [31], which is less than ideal for $p(\boldsymbol{\theta})$. We can justify the choice by the very good empirical results that have been achieved [11] and by the fact that we will use this criterion only for child model initialization and not for child model training. The Jeffrey's prior over mixing coefficients favors extreme estimates (0 or 1) more strongly than other priors (such as minimum entropy and negative Dirichlet), but this stronger component pruning is beneficial for this application.

Minimizing (16) with respect to $\pi(\mathcal{M})$ under the constraint that the priors $\pi(\mathcal{M})$ sum to 1, the following reestimation formulas are obtained [11]:

$$\hat{\pi}(\mathcal{M}) = \frac{\max\left\{0, -\frac{Q}{2} + \sum_{n=1}^{N} P(\mathcal{M}|\mathbf{t}_n)\right\}}{\sum_{\mathcal{M}'} \max\left\{0, -\frac{Q}{2} + \sum_{n=1}^{N} P(\mathcal{M}'|\mathbf{t}_n)\right\}}, \tag{17}$$

where component responsibilities $P(\mathcal{M}|\mathbf{t}_n)$ are determined by

$$P(\mathcal{M}|\mathbf{t}_n) = \frac{\pi(\mathcal{M})P(\mathbf{t}_n|\mathcal{M})}{\sum_{\mathcal{M}'} \pi(\mathcal{M}')P(\mathbf{t}_n|\mathcal{M}')}, \tag{18}$$

$$\pi(\mathcal{M}) = \frac{\sum_{n=1}^{N} P(\mathbf{t}_n|\mathcal{M})}{\sum_{\mathcal{M}'=1}^{A}\sum_{n=1}^{N} P(\mathbf{t}_n|\mathcal{M}')}. \tag{19}$$

Free parameters of the individual LTMs are fitted to the data ζ using the EM algorithm outlined in Section 3 applied to mixtures of LTMs.[5] This approach is not fully within the MML formalism, since there is no regularization of the LTM model parameters themselves: Instead, the mixing coefficients are regularized by (17). Note that LTMs corresponding to zero $\hat{\pi}(\mathcal{M})$ become irrelevant and, so, (17) effectively performs component annihilation [11].

4.2 The Algorithm

Given the training data $\zeta = \{\mathbf{t}_1, \mathbf{t}_2, \ldots, \mathbf{t}_N\}$, we use the MML approach to find the "appropriate" number of mixture component LTMs that "explain" ζ in a probabilistic manner. LTMs that are good probabilistic generating models of the data capture the data distribution well and, hence, yield "good" visualization plots.[6] To start the training process, we choose the maximum number of components A_{max} we are willing to consider at the next level. This can be set to a large value and the MML training procedure will select the optimal number of components no greater than A_{max}. If more components are needed, then the child model can be further refined at lower levels of the hierarchy. Then, the algorithm initializes the component LTMs by randomly selecting A_{max} points from ζ and applying the method described in Section 3.2. The selected A_{max} points act as centers of regions of interest in the data space. In other words, they play the role of vectors $z(\mathbf{c}_i)$ from Section 3.2.

As in [11], we adopt the component-wise EM (CEM) algorithm [9], i.e., rather than simultaneously updating all the LTMs, we first update the parameters $\boldsymbol{\Theta}^{(1)}$ of the first LTM (13), while parameters of the remaining LTMs are fixed, then we recompute the component responsibilities $\{P(\mathcal{M}|\mathbf{t}_n)\}$ (18) and mixture coefficients $\{\hat{\pi}(\mathcal{M})\}$ (17) for all components in the mixture. After this, we move to the second component, update $\boldsymbol{\Theta}^{(2)}$ in the same way, and recompute $\{P(\mathcal{M}|\mathbf{t}_n)\}$, $\{\hat{\pi}(\mathcal{M})\}$, etc., looping through all mixture components. If one of the component LTMs dies ($\hat{\pi}(\mathcal{M}) = 0$), redistribution of its probability mass to the remaining components increases their chance of survival. After convergence of CEM, we still have to check whether a shorter message length can be achieved by using a smaller number of mixture LTMs (down to $A = 1$).[7] This is achieved by iteratively killing off the weakest LTM (with the smallest $\hat{\pi}(\mathcal{M})$) and rerunning CEM until convergence. Finally, the

5. A mixture of LTMs can be considered a two-level hierarchical LTM. Mixture components are children of the *Root*.

6. This is a nontrivial issue since, while we can measure the quality of probabilistic models, e.g., via likelihood, there is no universal quality measure for visualization plots. But, intuitively, good probabilistic properties of a LTM mean that the projection manifold follows closely the data distribution and, so, the visualization plot is a "good" representation of the data distribution.

7. If we knew that the number of mixture components was no less than some number A_{min}, we would stop at $A = A_{min}$ [11].

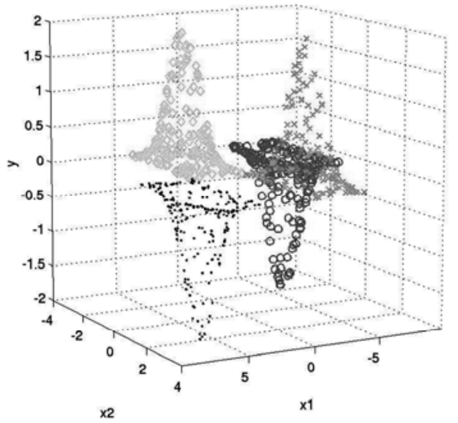

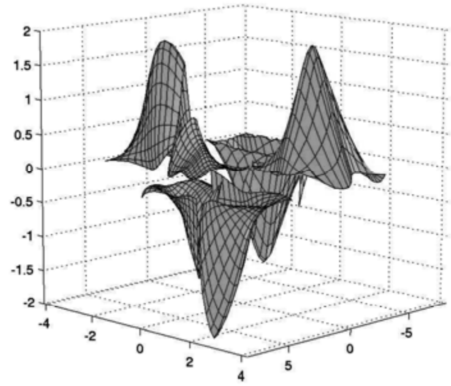

Fig. 2. (a) A two-dimensional manifold in data space. (b) Projection manifolds in data space of the second-level LTMs trained on the toy data.

winning mixture of LTMs is the one that leads to the shortest message length $\mathcal{L}(\boldsymbol{\theta}, \zeta)$ (16).

This training algorithm provides a very flexible approach to building a visualization model. The user can specify a different maximal number of child plots at each decision point, and there is no upper limit to the total number of plots in the hierarchy. Different parts of the hierarchy can be trained to different depths (i.e., there is no need for the tree to be balanced if that does not provide information). In addition, because each level of the hierarchy forms a probabilistic model of the data, it is possible for the user to "retract" decisions; if a set of child plots does not provide additional insight, that group can be removed, returning the tree to its previous optimal state.

To demonstrate this algorithm, we did an experiment on a toy data set of 800 points $\mathbf{t} = (t_1, t_2, t_3)^T$ lying on four two-dimensional manifolds ("humps") (see Fig. 2a). We associated the points in the four "humps" with four different classes, $\mathcal{C}_i$, $i = 1, 2, 3, 4$, having four different labels. After training[8] ($A_{max} = 10$), a 6-component mixture was constructed. Projection manifolds of the six LTMs are shown in Fig. 2b. Note that six child plots provide understandable subgroups of the data; and that the six projection manifolds closely approximate the four "humps"of the original generating manifold. The corresponding hierarchy of visualization plots can be seen in Fig. 3.

We stress that there is no contradiction between the number of components six in the final mixture of LTMs and the data set composed of four "humps." There is no driving force in the MML formalism to achieve this and this is not the point of our study. The important thing is that the MML method finds a good number of subplots so that the overall probability of the data set is high (good projections) and the mixture model is not too complex (unnecessarily high number of subplots). At the same time, the MML method *automatically* finds appropriate *positions* of the projection manifolds in the data space. Another advantage of using the MML criterion with the EM algorithm is that training is less sensitive to model initialization [11]. The criterion reduces the number of local optima in the error function (for example, removing the pathological cases where the variance of a component collapses to zero) and, so, the fact that EM (like all deterministic algorithms) only finds a local optimum is less of a problem.

8. We used LTMs with Gaussian noise model.

5 Semisupervised Learning of Visualization Hierarchies

The procedure for unsupervised learning of mixture models discussed in Section 4 becomes more complex for nodes (subplots) in hierarchical models at levels > 2. In this case, we should consider model responsibilities of parent nodes for the data points and these are recursively propagated as we incrementally build the hierarchy. So, (9) and (11) are used in hierarchical models instead of (18) used in the simple mixture case. Also, (6) is applied in place of (19).

The proposed system for constructing hierarchies of nonlinear visualization plots is similar to the one described in [27]. The important difference is that now, given a parent plot, its children are not always constructed in the interactive way by letting the user identify "regions of interest" for the subplots. In densely populated higher-level plots with many overlapping projections, this may not be possible. Instead, we let the user decide whether they want the children to be constructed in an interactive or unsupervised way.

In the unsupervised case, we use the MML technique to decide an "appropriate" number and approximate position of children LTMs. We collect data points from ζ for which the parent LTM has responsibility higher than a threshold Δ (in our experiments, Δ was set to[9] 0.9). We then run MML-based learning of *mixtures* of LTMs (Section 4.2) on this reduced data set. The resulting local mixture is viewed as an *initialization* for the full EM algorithm for training *hierarchies* of LTMs described in Section 3.1. This way, an "appropriate" number of LTMs is determined along with their initial locations.

It should be noted that, by using Jeffrey's prior, the approach suggested in [11] implies an improper Dirichlet prior (over the mixing coefficients) with negative parameters. As pointed out in [31], the use of the noninformative Jeffrey's prior in general raises problems from the Bayesian point of view. For instance, improper priors may lead to inadmissible estimates [26]. However, such priors have been extensively used mainly due to mathematical convenience: We do not have to compute the Fisher information

9. Other values for Δ, e.g., $\Delta = 0.8$, could have been used. However, the final local mixture of LTMs in the hierarchy is not very sensitive to the exact value of Δ, since this is just an initialization step, before running full EM for hierarchical LTM.

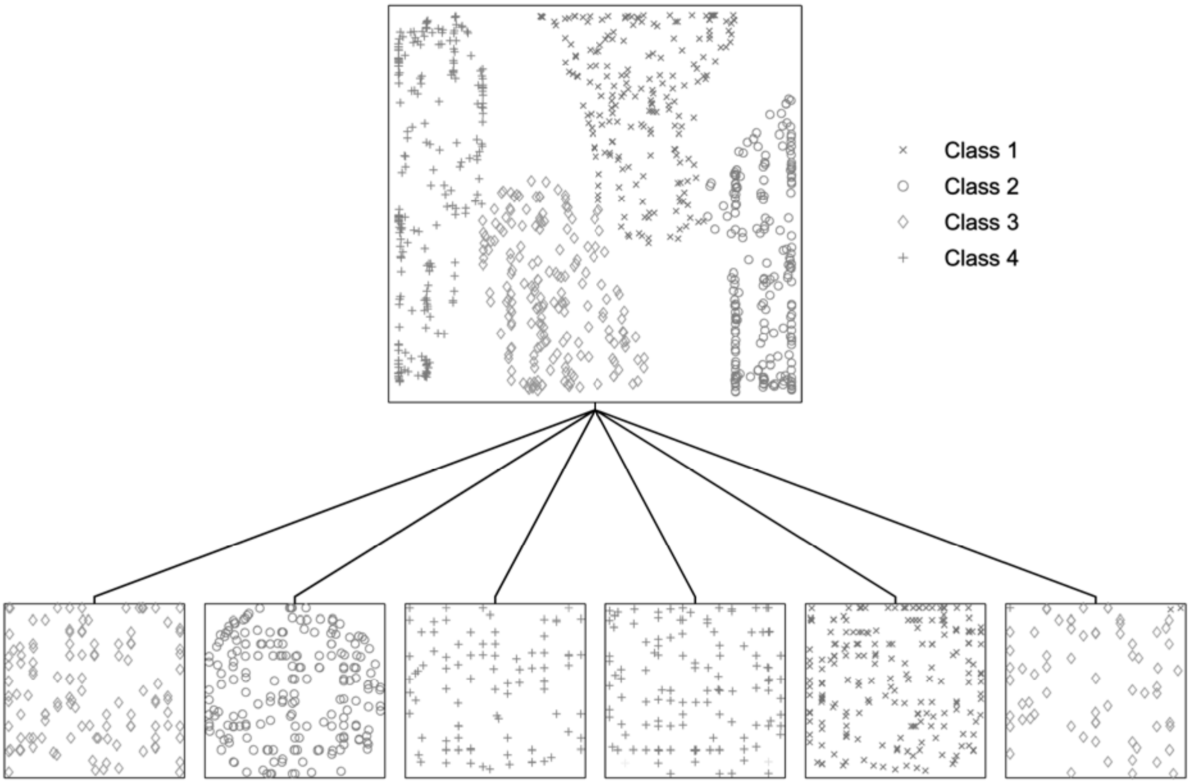

Fig. 3. Visualization of the toy data constructed with unsupervised MML.

matrix (typically, a computationally expensive step). Nevertheless, as we will demonstrate in the next section, we have experimentally found that for mixtures of LTMs, the use of Jeffrey's prior leads to sufficiently good initial estimates to be fed to the hierarchical EM described in Section 3.1. Moreover, the issue is less critical since the MML-based model selection is used solely to initialize the child models at higher levels of the hierarchy, while, typically, the user himself will refine the plots at lower levels of the hierarchy as in [27]. The Jeffrey's prior over the mixing coefficients favors strong component pruning, which is beneficial for our purposes.

5.1 Experiments

In this section, we illustrate the semisupervised hierarchical LTM visualization algorithm on three "real-world" data collections.

Although the algorithm is derived in a general setting in which individual LTMs $\mathcal{M}$ in the hierarchy can have different sets of latent points $x_k^{\mathcal{M}}$, $k = 1, 2, \ldots, K_{\mathcal{M}}$, and basis functions ϕ_j, $j = 1, 2, \ldots, M_{\mathcal{M}}$, in the experiments reported here, we used a common configuration for all models in the hierarchy. In particular, the latent space $\mathcal{H}$ was taken to be the two-dimensional interval $\mathcal{H} = [-1, 1] \times [-1, 1]$, the latent points $x_k^{\mathcal{M}} \in \mathcal{H}$ were positioned on a regular 15×15 square grid and there were 16 radial basis functions ϕ_j centered on a regular 4×4 square grid. As usual in the GTM literature, the basis functions were spherical Gaussians of the same width[10] $\sigma = 1.0$. We account for a bias term by using an additional constant basis function $\phi_0(x) = 1$, for all $x \in \mathcal{H}$. If the noise model in LTM is Gaussian, we always consider only spherical Gaussians, as in the original formulation of GTM [4]. Complete training equations for hierarchical GTM can be found in [27].

Note that in the interactive mode, the "centers" of the regions of interest are shown as circles labeled by numbers. These numbers determine the order of the corresponding child LTM subplots from left to right.

5.1.1 Image Segmentation Data

As the first example, we visualize image segmentation data obtained by randomly sampling patches of 3×3 pixels from a database of outdoor images. The patches are characterized by 18 continuous attributes and are classified into four classes: *cement + path*, *brickface + window*, *grass + foliage*, and *sky* (see [27]). The final visualization plot of hierarchical LTM with Gaussian noise model can be seen in Fig. 4. The *Root* plot contains clusters of overlapping projections. Six plots at the second level were constructed using the unsupervised MML technique ($A_{max} = 10$). Note that the second-level LTMs already separate the four classes fairly well and are interpretable enough to be analyzed further in the interactive mode. For example, we selected two and four "centers" for regions of interest (shown as circles) in the second and fifth level-two plots, respectively.

5.1.2 Text Data Set

Since our system is based on the LTM, it can deal with discrete data sets. As an illustration, we tested our system on a text-collection of 8,000 documents formed by 10 topic

10. The width of the basis functions is related to the "flexibility" of the generalized linear regression, $f_{\Theta}(x) = \Theta\phi(x)$, from the latent space to the data space. For a discussion on appropriate values for σ, see [4], [27].

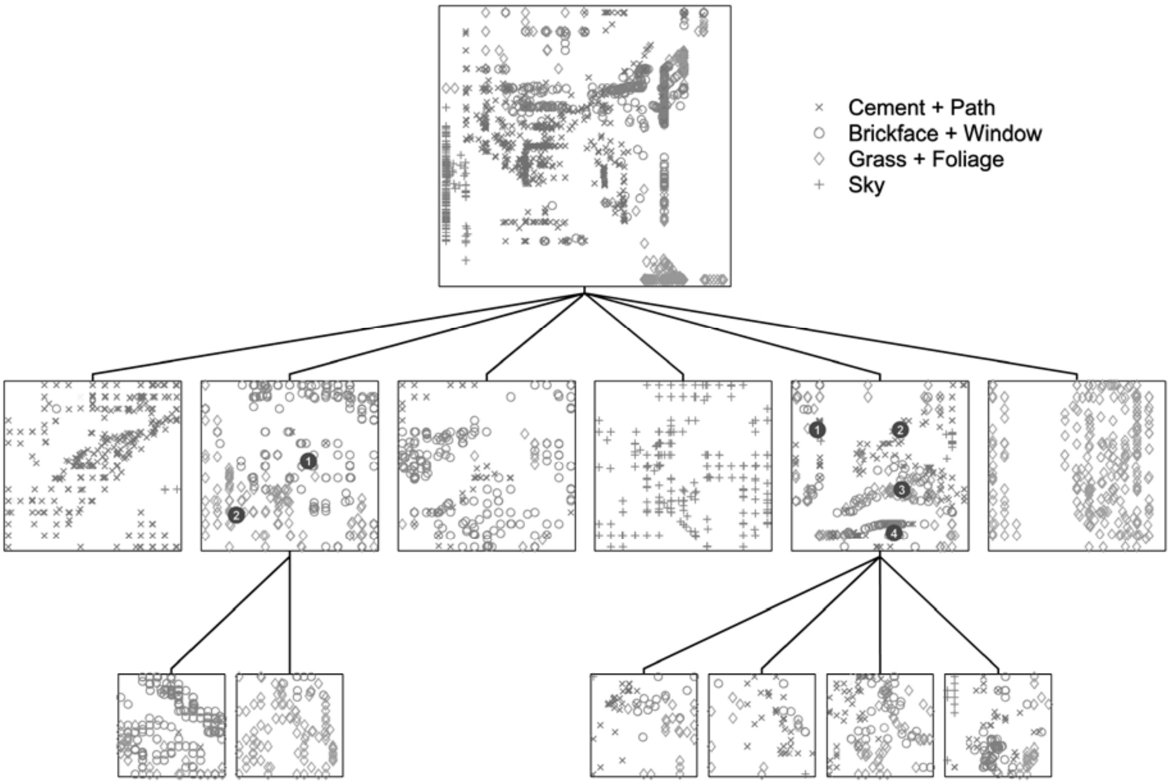

Fig. 4. Hierarchical visualization of the image segmentation data constructed in a semi-interactive way. Numbered circles represent user-selected locations for submodels.

classes from a newsgroup[11] text corpus. The documents were binary encoded over a dictionary of $D = 100$ words. The initial preprocessing, word-stemming, and removal of "stop-words" was done using the Bow toolkit.[12] To match the binary encoding, a Bernoulli noise model was employed, as a Gaussian would be inappropriate. Hence, a hierarchy of LTMs was used instead of HGTM.

The visualization plot generated in a semi-interactive way is shown in Fig. 5. The *Root* is extremely densely populated with highly overlapping data projections. After using the unsupervised MML technique ($A_{max} = 10$), a 4-component mixture of LTMs was obtained on the second level. Subclusters in these four level-two plots are decipherable. The user can then choose more detailed regions of interest by using the interactive mode. This is illustrated in the figure, but for complete class separation, more plots would be required.

As in [27], this system also includes the child-modulated ancestor plot technique, which can visualize the regions captured by a particular child LTM $\mathcal{M}$. This is done by modifying all the ancestor plots up to the *Root*, so that instead of the ancestor responsibilities, the responsibilities of the model $\mathcal{M}$, $P(\mathcal{M}|\mathbf{t}_n)$, are used in every plot on the path from $\mathcal{M}$ to *Root*. This improves the understanding of the relationships among subplots in the visualization hierarchy. In Fig. 6, we highlight the visualization plots which include the data points from the topic "sci.space," captured by the first model on the fourth-level.

11. http://www.cs.cmu.edu/~textlearning.
12. http://www-2.cs.cmu.edu/~mccalum/bow.

5.1.3 Protein Localization Site Data Set

In the last experiment, we visualize a data set of 1,484 proteins encoded as real-valued vectors.[13] The 6-dimensional data points[14] are classified into 10 classes (localization sites). The class names are shown in the legend of Fig. 7. Here, we demonstrate the application of the unsupervised MML technique at a lower level in the hierarchy.

We trained a four-level hierarchy of LTMs (Gaussian noise model) on the protein data and the resulting projections are displayed in Fig. 7. Again, the *Root* plot looks cluttered. Two plots at the second level were constructed using the unsupervised MML technique ($A_{max} = 10$). The first level-two plot is legible enough for the user to select the "centers" in the interactive mode (as shown in the figure). We used the MML algorithm as an initialization technique for constructing child plots of the second level-two plot ($A_{max} = 5$). Two resulting child plots included readable clusters.

Note that visualization plots for this data set do not provide a good separation, even at lower levels of the hierarchy. It follows that the features used to describe the data are not very discriminative with respect to the 10 binding site classes and the classes are highly overlapping. Our system enables the user to detect such situations by understanding the underlying data distribution. Our findings are confirmed by the poor classification

13. The data set can be downloaded from the UCI Machine Learning page: ftp://ftp.ics.uci.edu/pub/machine-learning-databases/yeast/.
14. The original data is 8-dimensional. Two of the dimensions are effectively constant and were removed.

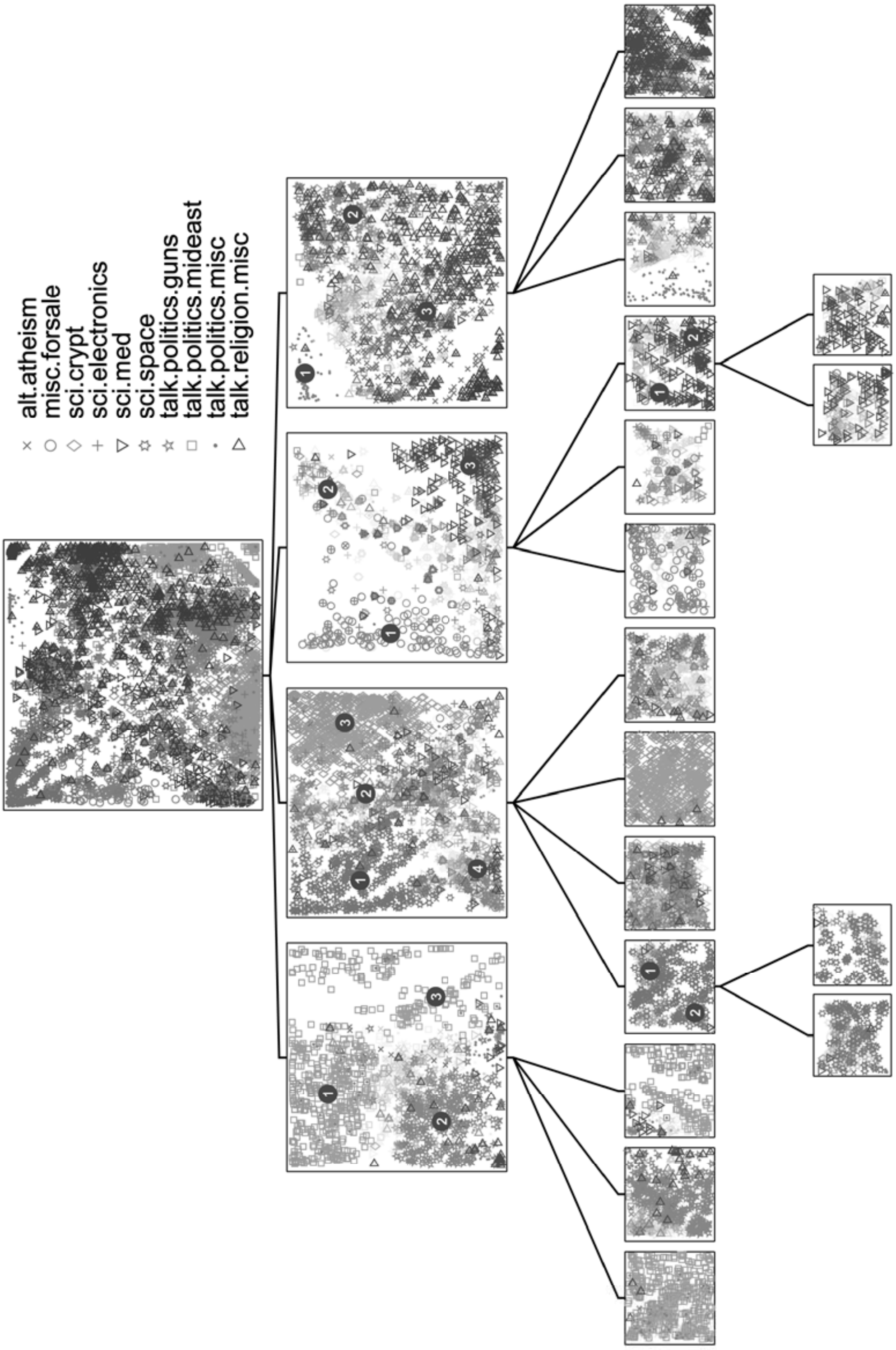

Fig. 5. Hierarchical visualization of the document data constructed in a semi-interactive way.

results (around 55 percent accuracy) obtained on this data set using various classification techniques [12].

5.2 Comparison

Although the primary focus of this paper is on automating the development of hierarchical models, it is also useful to compare our results with another hierarchical visualization technique. Interest in visualization of large multivariate data sets has been growing recently; as well as the generative approach taken by [7], [27] and this paper, more heuristic methods have also been developed [36], [19], [16]. We have selected the first of these, Interactive Hierarchical Displays (IHDs), as a benchmark for two main reasons: it is recent work that unifies several features of earlier techniques and it is the most closely related to our own in several

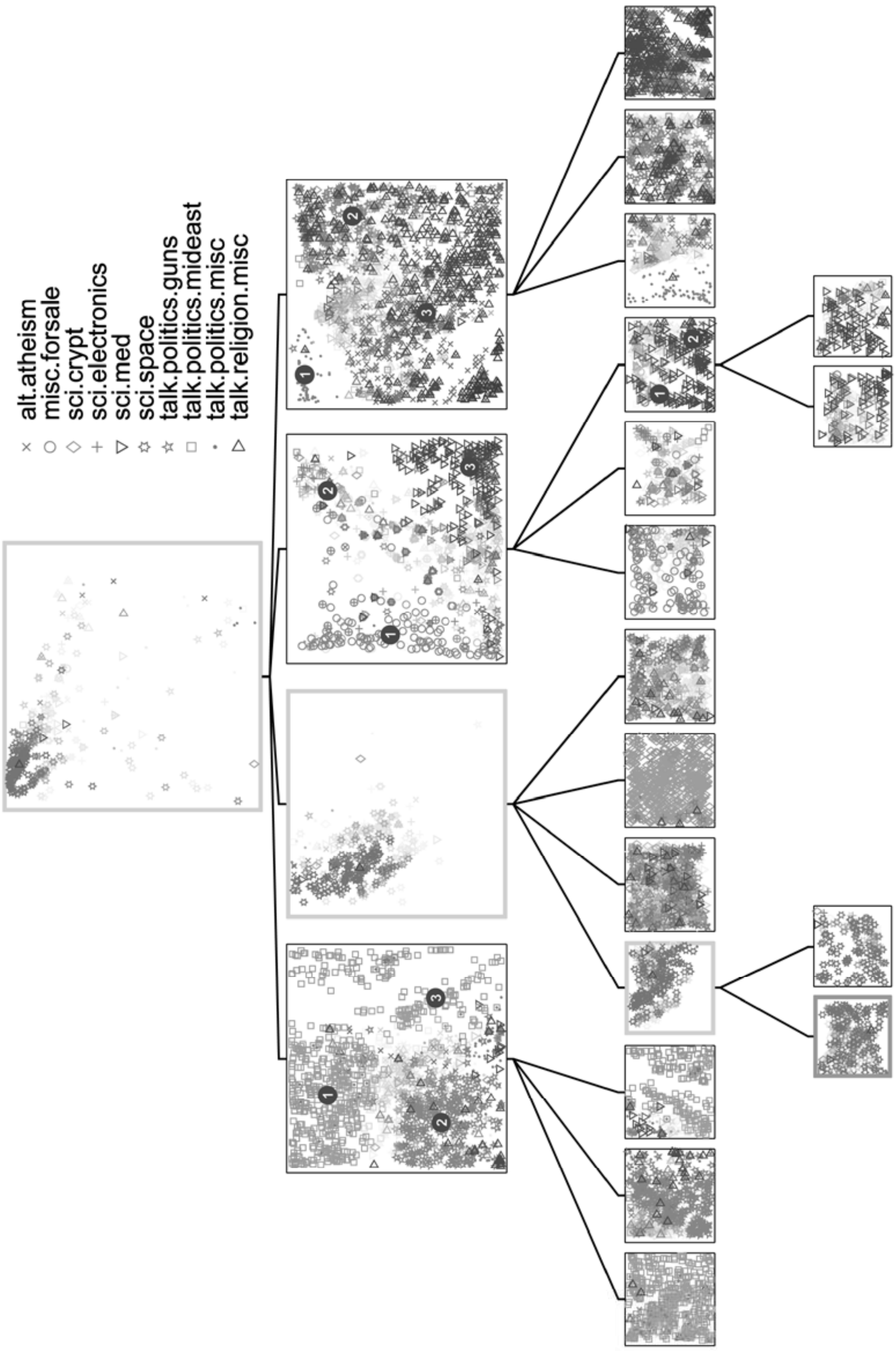

Fig. 6. Hierarchical visualization of the document data constructed in a semi-interactive way. The set of points captured by the first LTM at level 4 of the hierarchy is highlighted in the visualization plots of all its ancestors.

respects. It also has the advantage that an implementation is publicly available.[15]

Like HGTM, IHDs are designed to tackle the clutter problem faced by traditional multivariate visualization techniques when analyzing large data sets. The key strategy is to put fewer items on the screen. This is achieved by first constructing a hierarchical cluster tree. The tree can then be visualized at different levels of detail; the user specifies the point at which the tree is cut. Rather than showing all the datapoints, each cluster is displayed. The cluster is summarized by its mean with a band around it giving the minimum and maximum values in each variable of the cluster. This can be depicted using any multivariate

15. http://davis.wpi.edu/~xmdv.

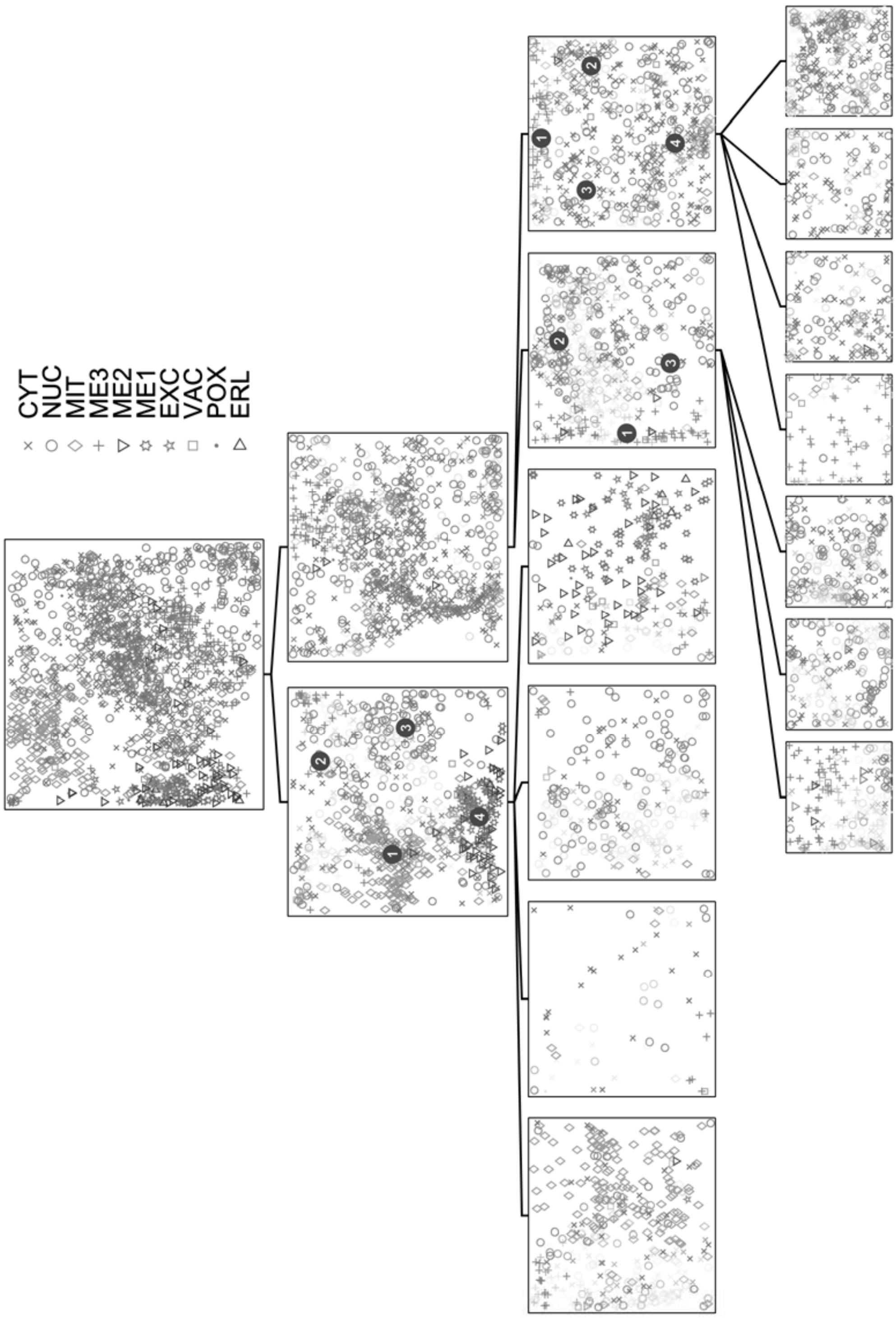

Fig. 7. Hierarchical visualization of the protein data set constructed in a semi-interactive way.

visualization technique that shows all the variables: [36] uses parallel coordinates [13], [34], star glyphs [24], scatterplot matrices and dimensional stacking [20]. A band is assigned the color of the cluster it represents. The strategy for this, called *proximity-based coloring* maps colors by cluster proximity based on the structure of the hierarchical tree. The strategy has the following properties:

- sibling clusters have similar colors and
- a parent cluster has a color within the range of its children's colors.

To create this map, it is necessary to impose a linear ordering on all the clusters.

Fig. 8 shows the result produced from hierarchical parallel coordinates when applied to the image segmentation data set. In current level, five clusters are captured. The mean points of individual clusters are mapped to a polyline across all the dimensions with a band indicating the range

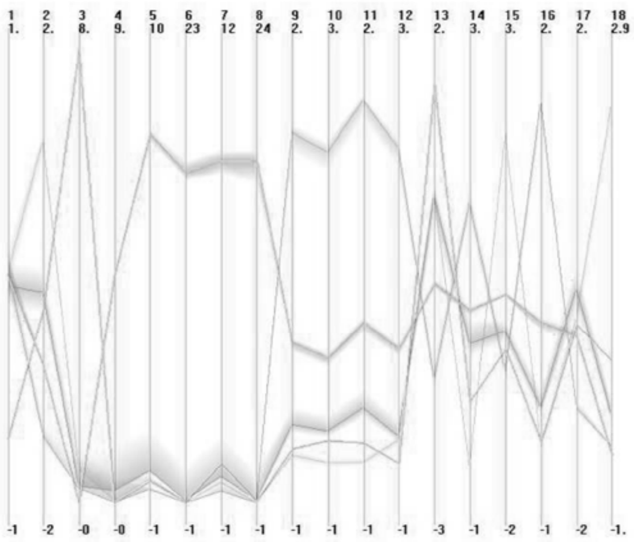

Fig. 8. Hierarchical parallel coordinates visualization plot using the image data set.

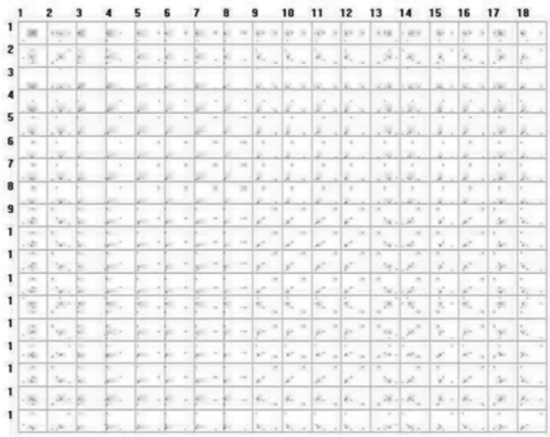

Fig. 10. Hierarchical scatterplot matrix visualization plot using the image data set.

of each cluster. This graph shows that it is difficult to see the shape of the clusters when compared with the results from HGTM (see Fig. 4). Fig. 9 displays hierarchical glyphs, where the mean values are used to generate the basic shape. Although it suggests the shape of each cluster, it is not clear which data points belong to it. In Fig. 10, a hierarchical scatterplot matrix is presented. Again, the points shown in the figure are the mean points of individual clusters. It is not clear which clusters are significant.

5.3 Discussion

IHDs are a useful means of visualizing hierarchical clusters. In [36], controlled experiments showed that most users could find more structure in data sets using IHDs rather than a single "flat" plot. They are a generic approach in that they can be used with any hierarchical tree clustering algorithm and any multivariate visualization that uses all the original variables.

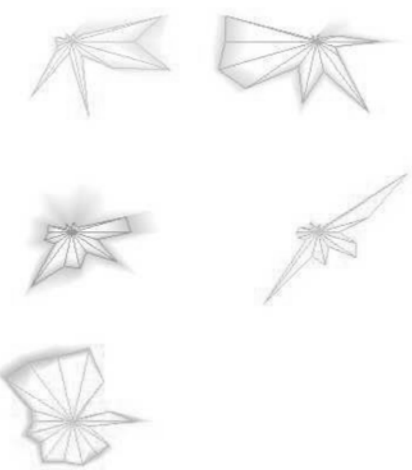

Fig. 9. Hierarchical star glyphs visualization plot using the image data set.

In contrast, our aim is more general: We want to represent the whole data set in two dimensions without loss of information. Only when this is not possible do we split the plot up. Consequently, the hierarchical trees that HGTM generates are usually much shallower and simpler than those produced by other hierarchical clustering methods. This allows the user to see the *whole* data set on a few plots which means they are less likely to get lost in multiple plots, but can still see the global picture.

Standard hierarchical clustering algorithms tend to perform poorly when there is a lot of noise in the data or when, as is often the case, the data is not split into well-separated clusters. In addition, they are usually based on heuristic distance measures. HGTM trees are a powerful method of clustering data and do not suffer from these disadvantages. In particular, they provide a *probabilistic density model* for the data, which brings many benefits (including principled automation of structure selection using Bayesian methods, as demonstrated in this paper). The fact that all the data is shown is also helpful; it allows the users to drill down into different regions and find out more about the *data* as well as the *clusters*. Users have expressed some concern that the coordinate system in the plots does not correspond with any meaningful variables. However, this drawback has been overcome by allowing them to specify regions where they can view the data locally using parallel coordinates.

Another important benefit of HGTM is that it projects the data onto a lower-dimensional space, which makes the plots much easier to interpret. HGTM has been applied to drug discovery data with more than 30 variables; at this size, multivariate visualization techniques like glyphs are very hard for users to understand. This two-dimensional representation also captures the relationships between clusters (which is very important to develop real understanding of the data); IHDs use a one-dimensional representation of intercluster relationships (the proximity-based coloring) that is necessarily less rich in expressive power.

IHDs are a display technique, so the only time consuming aspect is the hierarchical clustering algorithm. HGTM has an efficient EM algorithm: It takes 2-3 minutes to train a model for a data set of 1,000 examples and see 15 variables on a "standard" 1GHz PC. The automated

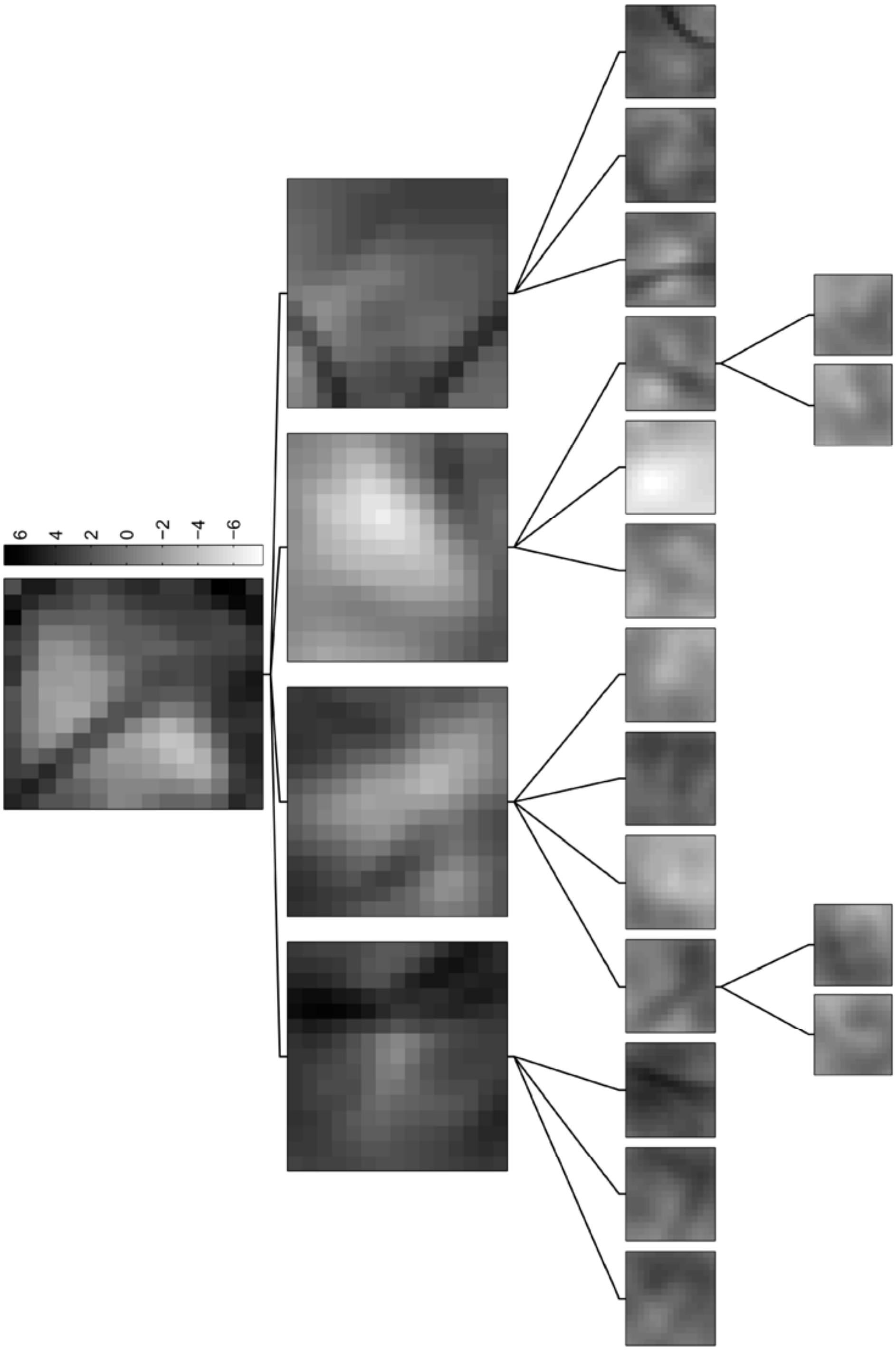

Fig. 11. Plots of magnification factors (log2-scaled) in the hierarchy of LTMs fitted on the document data.

initialization algorithm takes somewhat longer since there is a need to train models of several different structures at each level: the image segmentation and protein data sets required in the order of 10 minutes to train. The text data set, with 8,000 examples and 100 variables, takes rather longer: in the order of two hours. It is worth noting that these times are based on a program written using the MATLAB mathematical toolkit; an implementation in a 3GL such as C would normally be around twice as fast. Once the model is trained, the user can interact with the plot with no time delays.

6 Local Magnification Factors of the Latent Trait Manifolds

In this section, we first briefly review the notion of local magnification factors for the original GTM [6]. We then rederive the formula for computing magnification factors for the more general LTM.

The term "magnification factor" [6] refers to the degree of stretching or compression of the latent space when embedded into the data space. Previous experience has indicated that magnification factors are a useful tool for interpreting 2D nonlinear visualization plots. For example, projections of well-separated dense clusters of data points will occupy compressed regions on the visualization plot (small magnification factors), separated by a band of highly stretched area (high magnification factors).

Let us consider the Cartesian coordinate system defined on the latent space and the mapping of this space to a curvilinear coordinate system defined on the manifold embedded in the data space. The local magnification factor corresponding to a point x_0 in the latent space can be defined as the ratio between the area of an infinitesimal rectangle in the latent Cartesian space and the area generated by mapping it through (3) on the projection manifold. This ratio is equal to $\sqrt{|S(\boldsymbol{x}_0)|}$, where $|S(\boldsymbol{x}_0)|$ is the determinant of the metric tensor $S = \boldsymbol{\Gamma}^T\boldsymbol{\Gamma}$, where $\boldsymbol{\Gamma}$ denotes the Jacobian of the mapping (3) at $\boldsymbol{x}_0$. For GTM, since $\boldsymbol{b}(.)$ is identity function, $\boldsymbol{\Gamma}$ evaluates as $\boldsymbol{\Theta}V$, where V is the $M \times L$ matrix $\left(\frac{\partial \phi_m(\boldsymbol{x})}{\partial x_l}{}_{|\boldsymbol{x}=\boldsymbol{x}_0}\right)_{m=1,\dots,M,l=1,\dots,L}$.

For the Latent Trait Models, we have

$$\boldsymbol{\Gamma} = \frac{\partial \boldsymbol{z}(\boldsymbol{x}_0)}{\partial \boldsymbol{x}} = \frac{\partial \boldsymbol{b}(\boldsymbol{\Theta}\phi(\boldsymbol{x}_0))}{\partial \boldsymbol{x}} = \boldsymbol{F\Theta V}, \tag{20}$$

where the $D \times D$ matrix

$$\boldsymbol{F} = \left(\frac{b_{d'}(\boldsymbol{y})}{\partial y_d}{}_{|\boldsymbol{y}=\boldsymbol{\Theta}\phi(\boldsymbol{x}_0)}\right)_{d'=1,\dots,D,d=1,\dots,D}$$

is the Fisher information matrix of the noise distribution. Indeed, if the noise model is Gaussian, F turns out to be the identity matrix. With the choice of RBF nonlinearities for $\phi(\cdot)$, the (l,m)th element of the matrix V is $v_{l,m} = -\phi_m(\boldsymbol{x}_0)(x_l - c_{m,l})\sigma^{-2}$, where $c_{m,l}$ denotes the lth coordinate of the radial basis center corresponding to the mth basis function and σ is the width of the RBF functions.

In summary, the magnification factor associated with a latent space point $\boldsymbol{x}_0$ is

$$\sqrt{|\boldsymbol{V}^T 0^T \boldsymbol{F}^T \boldsymbol{F\Theta V}|}. \tag{21}$$

It is easy to see that this formula differs from the one derived in [6] for the original GTM by the presence of the matrix $\boldsymbol{F}^T\boldsymbol{F}$, which reduces to identity in the case of Gaussian noise. So, the formula for computing magnification factors for GTM derived in [6] is recovered in the special case of (21), when the noise is Gaussian.

Note also that in all independent noise models, this matrix will be diagonal; therefore, the increase in computational complexity will not be significant. However, this is not the case for the multinomial trait model (as can be seen in Appendix A.3).

As an example, we show in Fig. 11 the magnification factor plots (log-scaled) for the projection hierarchy of the text data set in Fig. 5. In general, dark bands in the plots indicate well-separated clusters of points in the data space. For example, there is a dark band slightly left of the center of the 11th level-three model. The band divides different topics in the data space. From the corresponding model in Fig. 5, we see that the left region mostly involves topic

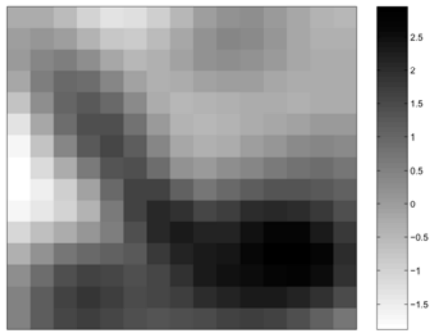

Fig. 12. A rescaled visualization plot of magnification factors for the fourth LTM at level 3 in the hierarchy shown in Fig. 11.

"talk.politics.misc," and the right region contains a mixture of topics.

As an example of detailed analysis of magnification factors, we focus on the fourth level-three LTM model in Fig. 11. The corresponding projection plot in Fig. 5 contains mostly documents from a single topic, "sci.space." An enlarged (locally-scaled) view of the magnification factor plot is presented in Fig. 12. There is a dark band around the diagonal line of the plot. Hence, we infer that documents on either side of the band correspond to different clusters and that a change of *subtopic* occurs. The list of five most probable dictionary words for each latent space centre of the corresponding LTM is shown in Fig. 13. With reference to Fig. 12, two clusters can be found on each side of the separating band. Key words for each latent space center inside the region bounded by the solid border are completely the same and have the same ordering. They appear to refer to documents relating to space shuttle launches, while key words inside the region with the dashed border seem to be associated with articles concerning space orbits.

7 Conclusion

In this paper, we have presented a general system for hierarchical visualization of large data sets which may be of either continuous or discrete type. We also derived formulas for magnification factors in latent trait models. The proposed system gives the user a choice of initializing the child plots of the current plot in either *interactive*, or *automatic* mode. This latter feature is particularly useful when the user has no idea how to choose the area of interest due to highly overlapping dense data projections. We have evaluated this system on three real world data sets and compared the results with an existing method for hierarchical visualization. In many problems, particularly where there are not clearly defined and separated clusters of data, hierarchical LTMs offer significant benefits.

The system can be used in many different fields, such as document data mining, telecommunications, bioinformatics, market-basket analysis, or information retrieval. We are currently developing this system further to provide more user feedback during the data exploration process and to combine visualization with localized modeling (for example, to predict properties of chemical compounds).

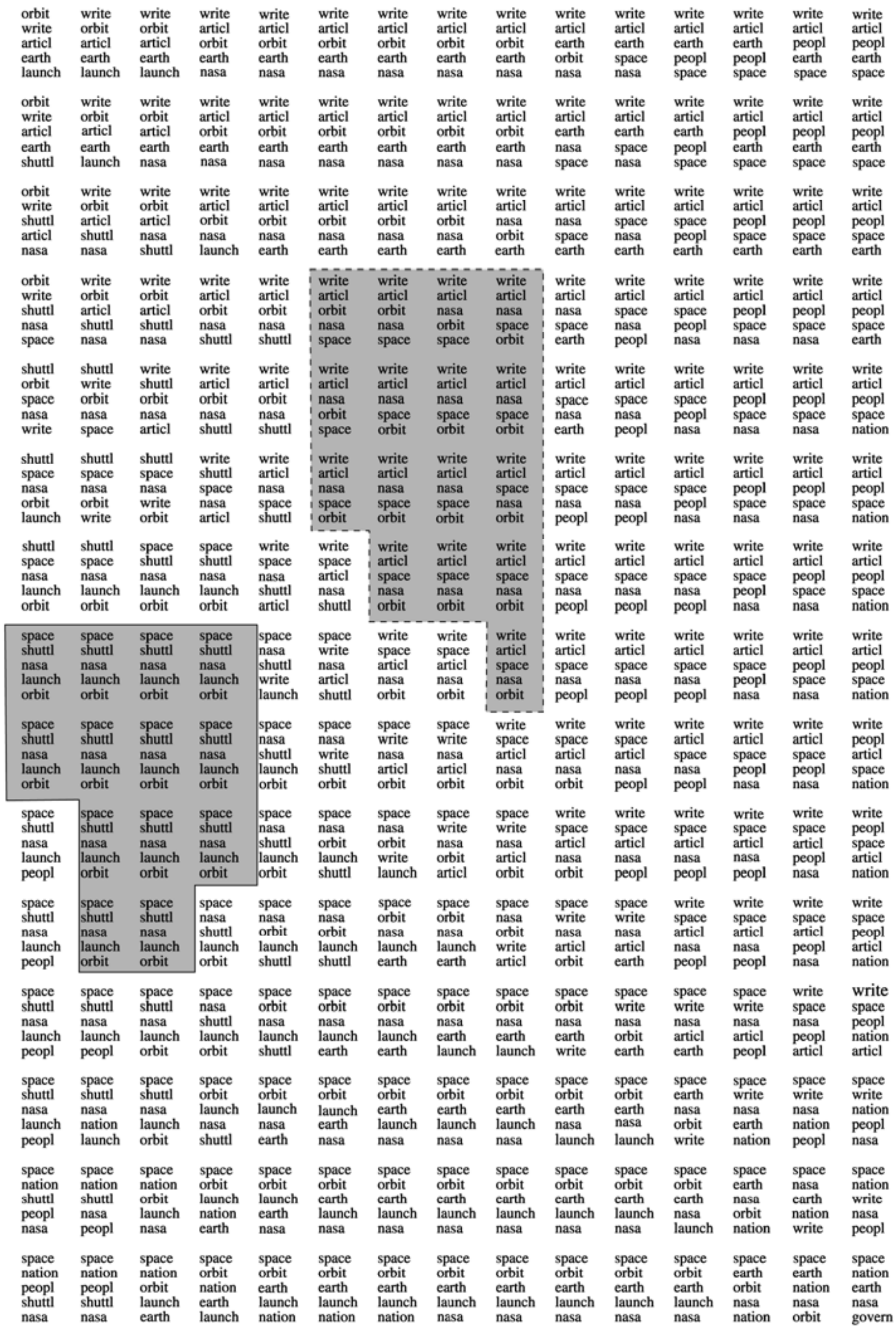

Fig. 13. The most probable words formed in each of the 15 by 15 latent grid points by the Bernoulli latent trait model obtained in the experiments on text documents data.

Appendix

Quantities Required for Computing Magnification Factors in the Reported Experimental Settings

The exact form of the matrices F is dependent on the specific noise-model being employed. These quantities require the computation of the first derivatives of the inverse link function $b()$. In this Appendix, we will provide the expressions for those members of the exponential model family which have been employed in the reported experimental settings.

A.1 Independent Gaussian Noise Model

The Gaussian model is the only member of the exponential family of distributions which is characterised by a quadratic cumulant function

$$B_t(\mathbf{y}) = \frac{1}{2} y_t^2. \tag{22}$$

Therefore, it has a linear inverse-link function and higher derivatives vanish.

$$b_{t'}(\mathbf{y}) = y_{t'}, \tag{23}$$

$$\frac{\partial b_{t'}(\boldsymbol{y})}{\partial y_t} = 0. \tag{24}$$

A.2 Independent Bernoulli Noise Model

In the case of the Bernoulli model, the cumulant function has the following form:

$$B_t(\boldsymbol{y}) = \log(1 + exp(y_t)). \tag{25}$$

The required derivatives are then computed as follows:

$$b_{t'}(\boldsymbol{y}) = \frac{\exp(y_{t'})}{1 + \exp(y_{t'})}, \tag{26}$$

$$\frac{\partial b_{t'}(\boldsymbol{y})}{\partial y_t} = \begin{cases} 0 & t \neq t' \\ b_t(\boldsymbol{y})(1 - b_t(\boldsymbol{y})) & t = t'. \end{cases} \tag{27}$$

It can be seen that for independent noise models, the Fisher information matrix $\boldsymbol{F}$ is diagonal.

A.3 Multinomial Noise Model

The multinomial distribution is identified by the following cumulant function:

$$B(\boldsymbol{y}) = \log\left(\sum_{t=1:T} exp(y_t)\right). \tag{28}$$

Accordingly, the derivatives are given by

$$b_{t'}(\boldsymbol{y}) = \frac{\exp(y_{t'})}{\sum_{t''=1}^{T} \exp(y_{t''})}, \tag{29}$$

$$\frac{\partial b_{t'}(\boldsymbol{y})}{\partial y_t} = \begin{cases} -b_{t'}(\boldsymbol{y}) b_t(\boldsymbol{y}) & t \neq t' \\ b_{t'}(\boldsymbol{y}) - b_{t'}(\boldsymbol{y}) b_t(\boldsymbol{y}) & t = t'. \end{cases} \tag{30}$$

Acknowledgments

This research has been funded by BBSRC grant 92/BIO12093 and Pfizer Central Research. Part of the work has been done while Ata Kabán was supported by resource, The Council for Museums, Archives, and Libraries, Grant Number RE/092, at the University of Paisley. The experiments were carried out with the NETLAB neural network toolbox, available from http://www.ncrg.aston.ac.uk/netlab. The hierarchical graph plots were based on the PhiVis software http://www.ncrg.aston.ac.uk/PhiVis, and the authors are grateful to Michael Tipping for allowing us to use his software. Yi Sun would like to thank Mario A.T. Figueiredo for providing his software. Finally, the authors are most grateful to the anonymous referees for their valuable and insightful comments on the manuscript.

References

[1] F. Aurenhammer, "Voronoi Diagrams—Survey of a Fundamental Geometric Data Structure," *ACM Computing Surveys*, vol. 3, pp. 345-405, 1991.

[2] O. Barndorff-Nielsen, *Information and Exponential Families in Statistical Theory*. Wiley, 1978.

[3] J. Bernardo and A. Smith, *Bayesian Theory*. Chichester, U.K.: J. Wiley & Sons, 1994.

[4] C.M. Bishop and M. Svensén, and C.K.I. Williams, "GTM: The Generative Topographic Mapping," *Neural Computation*, vol. 10, no. 1, pp. 215-235, 1998.

[5] C.M. Bishop and M. Svensén, and C.K.I Williams, "Developments of the Generate Topographic Mapping," *Neurocomputing*, vol. 21, pp. 203-224, 1998.

[6] C.M. Bishop and M. Svensén, and C.K.I. Williams, "Magnification Factors for the GTM Algorithm," *Proc. IEE Fifth Int'l Conf. Artificial Neural Networks*, pp. 64-69, 1997.

[7] C.M. Bishop and M.E. Tipping, "A Hierarchical Latent Variable Model for Data Visualization," *IEEE Trans. Pattern Analysis and Machine Intelligence*, vol. 20, no. 3, pp. 281-293, 1998.

[8] D.M. Boulton and C.S. Wallace, "An Information Measure for Hierarchic Classification," *Computer J.*, vol. 16, no. 3, pp. 254-261, 1973.

[9] G. Celeux and S. Chrétien, F. Forbes, and A. Mkhadri, "A Component-Wise EM Algorithm for Mixtures," *J. Computational and Graphical Statistics*, vol. 10, pp. 699-712, 2001.

[10] A.P. Dempster and N.M. Laird, and D.B. Rubin, "Maximum Likelihood from Incomplete Data via the EM Algorithm," *J. Royal Statistical Soc., Series B*, vol. 39, pp. 1-38, 1977.

[11] M. Figueiredo and A.K. Jain, "Unsupervised Learning of Finite Mixture Models," *IEEE Trans. Pattern Analysis and Machine Intelligence*, vol. 24, pp. 381-396, 2002.

[12] P. Horton and K. Nakai, "A Probabilistic Classification System for Predicting the Cellular Localization Sites of Proteins," *Intelligent System in Molecular Biology*, vol. 4, pp. 109-115, 1996.

[13] A. Inselberg and B. Dimsdale, "Parallel Coordinates: A Tool for Visualizing Mulitdimensional Geometry," *Proc. Visualisation '90*, pp. 361-78, 1990.

[14] A. Kabán and M. Girolami, "A Combined Latent Class and Trait Model for the Analysis and Visualization of Discrete Data," *IEEE Trans. Pattern Analysis and Machine Intelligence*, vol. 23, no. 8, pp. 859-872, Aug. 2001.

[15] A. Kabán, P. Tiňo, and M. Girolami, "A General Framework for a Principled Hierarchical Visualisation of Multivariate Data," *Proc. Third Int'l Conf. Intelligent Data Eng. and Automated Learning (IDEAL '02)*, pp. 17-23, 2002.

[16] D.A. Keim, H.P. Kriegel, and M. Ankerst, "Recursive Pattern: A Technique for Visualizing Very Large Amounts of Data," *Proc. Sixth IEEE Visualization 1995 Conf. (VIS '95)*, pp. 279-286, 1995.

[17] T. Kohonen, "The Self-Organizing Map," *Proc. IEEE*, vol. 78, no. 9, pp. 1464-1479, 1990.

[18] T. Kohonen, *Self-Organizing Maps*. Berlin: Springer-Verlag, 1999.

[19] Y. Koren and D. Harel, "A Two-Way Visualization Method for Clustered Data," *Proc. Ninth ACM SIGKDD Int'l Conf. Knowledge Discovery and Data Mining*, pp. 589-594, 2003.

[20] J. LeBlanc, M.O. Ward, and N. Wittels, "Exploring *n*-Dimensional Databases," *Proc. Visualisation '90*, pp. 230-237, 1990.

[21] P. McCullagh and L. Nelder, *Generalized Linear Models*. Chapman and Hall, 1985.

[22] R. Miikkulainen, "Script Recognition with Hierarchical Feature Maps," *Connection Science*, vol. 2, pp. 83-101, 1990.

[23] E. Pampalk, W. Goebl, and G. Widmer, "Visualising Changes in the Structure of Data for Exploratory Feature Selection," *Proc. 2003 ACM SIGKDD Int'l Conf. Knowledge Discovery and Data Mining (KDD '03)*, P. Domingos et al., eds., pp. 157-166, 2003.

[24] W. Ribarsky, E. Ayers, J. Eble, and S. Mukherjea, "Glyphmaker: Creating Customized Visualization of Complex Data," *Computer*, vol. 27, vol. 7, pp. 57-64, 1994.

[25] S.J. Roberts and C. Holmes, and D. Denison, "Minimum-Entropy Data Partitioning Using Reversible Jump Markov Chain MonteCarlo," *IEEE Trans. Pattern Analysis and Machine Intelligence*, vol. 23, pp. 909-914, 2001.

[26] C. Stein, "Approximation of Improper Prior Measures by Proper Probability Measures," Bernoulli, Bayes, Laplace Festschrift. (J. Neyman and L. LeCam, eds.)., Berlin: Springer, pp. 217-240, 1965.

[27] P. Tiňo and I.T. Nabney, "Hierarchical GTM: Constructing Localized Nonlinear Projection Manifolds in a Principled Way," *IEEE Trans. Pattern Analysis and Machine Intelligence*, vol. 24, pp. 639-656, 2002.

[28] C.S. Wallace and D.L. Dowe, "Minimum Message Length and Kolmogorov Complexity," *The Computer J.*, vol. 42, pp. 270-283, 1999.

[29] C.S. Wallace and D.M. Boulton, "An Information Measure for Classification," *The Computer J.*, vol. 11, no. 2, pp. 185-194, 1968.

[30] C.S. Wallace and D.L. Dowe, "Intrinsic Classification by MML—the Snob Program," *Proc. Seventh Australian Joint Conf. Artificial Intelligence*, C. Zhang et al., eds., World Scientific, pp. 37-44, 1994.

[31] C.S. Wallace and D.L. Dowe, "Refinements of MDL and MML Coding," *Computer J.*, vol. 42, no. 4, pp. 330-337, 1999.
[32] C.S. Wallace and D.L. Dowe, "MML Clustering of Multi-State, Poisson, Von Mises Circular and Gaussian Distributions," *Statistics and Computing*, vol. 10, pp. 73-83, 2000.
[33] C.S. Wallace and P.R. Freeman, "Estimation and Inference by Compact Coding," *J. Royal Statistical Soc., series B*, vol. 49, pp. 240-265, 1987.
[34] E.J. Wegman, "Hyperdimensional Data Analysis Using Parallel Coordinates," *J. Am. Statistical Assoc.*, vol. 411, no. 85, p. 664, 1990.
[35] R. Wolke and H. Schwetlick, "Iterative Reweighted Least Squares: Algorithms, Convergence Analysis, and Numerical Comparisons," *SIAM J. Scientific and Statistical Computing*, vol. 9, no. 5, pp. 907-921, 1999.
[36] J. Yang, M.O. Ward, and E.A. Rundensteiner, "Interactive Hierarchical Displays: A General Framework for Visualisation and Exploration of Large Multivariate Data Sets," *Computers and Graphics J.*, vol. 27, pp. 265-283, 2002.

Ian T. Nabney studied mathematics at Oxford University (BA degree, 1985) and Cambridge University (PhD degree, 1989). He then spent five years with Logica at their research lab, where he developed a wide range of neural network applications. In 1995, he was appointed as a lecturer in the Department of Computer Science and Applied Mathematics at Aston University and, in 2004, he was promoted to a chair in computer science. His research spans both the theory and applications of neural networks and other pattern recognition techniques. Much of his work is inspired by industrial problems in bioinformatics, biosignal processing, and financial forecasting. He has put his experience of software engineering to good use by developing the Netlab toolbox for pattern recognition.

Yi Sun studied thermal energy engineering and received the BSc degree from the University of Science & Technology Beijing (USTB), China. In 1999, she studied at Aston University and received the PhD degree in 2003. She works currently as a research fellow in the neural network group at the University of Hertforshire, United Kingdom. Her current research interests are probabilistic modeling, data visualization, pattern classification and clustering, and neural computation models of cognitive and psychological processes.

Peter Tiňo studied at Slovak University of Technology and received the PhD degree (1997) from the Slovak Academy of Sciences. He worked at the NEC Research Institute in Princeton, New Jersey, the Austrian Research Institute for Artificial Intelligence in Vienna, Austria, and Aston University in Birmingham, United Kingdom. He is currently a lecturer in the School of Computer Science, the University of Birmingham, United Kingdom. His scientific interests are probabilistic modeling and visualization of structured data, dynamical systems, and fractal analysis.

Ata Kabán received the BSc degree with honors (1999) in computer science from the University "Babes-Bolyai" of Cluj-Napoca, Romania, and the PhD degree in computer science (2001) from the University of Paisley, United Kingdom. She is a lecturer in the School of Computer Science at the University of Birmingham. Her current interests concern probabilistic modeling, machine learning, and their applications to automated data analysis. She has been a visiting researcher at Helsinki University of Technology (June-December 2000, Summer of 2003). Prior to her career in computer science, she received the BA degree in musical composition (1994) and the MA (1995) and PhD (1999) degrees in musicology from the Music Academy "Gh. Dima" of Cluj-Napoca, Romania.